ELSEVIER

Journal of Biomechanics 31 (1998) 453–462

JOURNAL OF BIOMECHANICS

Analysis of 3D transient blood flow passing through an artificial aortic valve by Lattice–Boltzmann methods

M. Krafczyk[a,*], M. Cerrolaza[b], M. Schulz[a], E. Rank[a]

[a]*Lehrstuhl für Bauinformatik, Civil Engineering Department, Tu München Arcisstr. 21, D-80290 Munich, Germany*
[b]*Bioengineering Center, Faculty of Engineering, Central University of Venezuela, PO Box 50.361, Caracas 1050-A, Venezuela*

Received in final form 20 October 1997

Abstract

The development of flow instabilities due to high Reynolds number flow in artificial heart valve geometries inducing high strain rates and stresses often leads to hemolysis and related highly undesired effects. Geometric and functional optimization of artificial heart valves is therefore mandatory. In addition to experimental work in this field it is meanwhile possible to obtain increasing insight into flow dynamics by computer simulation of refined model problems. After giving an introductory overview we report the results of the simulation of three-dimensional transient physiological flows in *fixed* geometries similar to a CarboMedics bileaflet heart valve at different opening angles. The visualization of emerging complicated flow patterns gives detailed information about the transient history of the systems dynamical stability. Stress analysis indicates temporal shear stress peaks even far away from walls. The mathematical approach used is the Lattice–Boltzmann method. We obtained reasonable results for velocity and shear stress fields. The code is implemented on parallel hardware in order to decrease computation time. Finally, we discuss problems, shortcomings and possible extensions of our approach.

Keywords: Blood flow; Artificial heart valve; Lattice–Boltzmann method

Nomenclature

f	probability distribution function
$\mathbf{e}_i$	discrete velocity vector
Ω	collision operator
τ	microscopic relaxation parameter
c_s	speed of sound
ν	kinematic viscosity
ρ	density
$\mathbf{u}$	velocity
σ_{xz}	shear stress
p	pressure
t	time
$\mathbf{x}$	position vector

1. Introduction

Many important aspects of haemodynamic aortic blood flow have been investigated in experimental studies (Skalak, 1982; Farahifar et al., 1985; Chandran et al., 1983, 1985; Rosseau et al., 1984; Sallam et al., 1976; Tillman et al., 1984; Yoganathan et al., 1979; Woo et al., 1986) but sometimes these studies lack spatial resolution, have problems analyzing transient phenomena or partially lack the detailed observation of theoretically interesting variables crucial for extended theoretical modeling because they are hard to measure. These partial drawbacks and limitations have suggested that numerical methods could be of significant help when analyzing the dynamics of flowing blood. Numerical simulation has indeed led to a better understanding of blood flow behavior and has allowed medical hemodynamicists to gain an improved understanding of the behavior of containing structures (vessels and heart) as well as the contained flow (blood). Both of these structures can now be investigated in more detail, especially considering the influence of transient effects. The four different cardiac valves are:

- Atrium-ventrical (intracardiac): three-cusps and mitral.
- Ventrical-arterials: aortic and lung valves.

The function of these valves is to regulate the biologic fluid flow in a continuous manner and to avoid the ebb of the blood ejected by the heart (see Braunwald, 1992;

*Corresponding author. E-mail: kraft@server.inf.bauwesen.tu-muenchen.de.

0021-9290/98/$19.00
PII: S0021-9290(98)00036-0

Bardet, 1983; Drobinsky et al., 1992). An important malfunction of these processes can be identified as the pathological state known as thrombosis resulting from high shear stresses or increased coagulation due to blood stagnancy in contact with the artery walls. Basically, both phenomena will produce coagulated masses of blood, which flow through the cardiovascular system until they reach a small cross-section vessel, causing the undesirable obstruction. Similarly to blood flow problems caused by stenosis many long-time problems in valve hemodynamics are due to the intrinsic non-linear weakly turbulent flow dynamics and the resulting shear stress. Yet an improvement of valve design requires a detailed understanding of these system properties and substantial further experimental research. As *in vivo* experimental investigations are extremely difficult, major progress has to be obtained by *in vitro* measurements and numerical simulations. In the field of computational and numerical analysis, several works can be found in the technical literature investigating steady (e.g. Gokhale et al., 1978; Cerrolaza et al., 1997), pulsatile (e.g. Imaeda et al., 1980; Sikarskie et al., 1979) and turbulent blood flows (e.g. Ştevenson et al., 1985). Most of the simulations described in the literature used FEM, FV or FD schemes to discretize the equations under investigation, usually the Navier–Stokes equation coupled with a continuity equation. Ideally, however, one would like to analyze a fully transient 3D model including moving leaflets. Yet reliable simulation of the 3D transient flows for a peak Reynolds number well above 1000 is still a challenge for todays state-of-the art methods and computers, even if a proper fluid–solid interaction between the valve leaflets and the fluid, the fluid and the wall of the aorta as well as non-Newtonian stress–strain relations are *not* included.

The present work investigates the alterations produced in the blood flow when an aortic artificial valve is introduced into the blood stream. The evolving velocity patterns and shear stresses of blood flow passing through the device are studied and discussed. The main novelty of the approach in this work is the use of a Lattice–Boltzmann model to simulate blood flows.

2. Numerical method

For decades the scientific community has struggled to develop and optimize suitable algorithms like finite volume, finite element, spectral, or finite difference methods to simulate high Reynolds number Navier–Stokes problems. Apart from these mainstream approaches the last years have seen further attempts to model flow problems on particle-based methods such as the so-called Lattice-gas method. A LG consists of a large ensemble of idealized particles living on the nodes of a grid of given symmetry which undergo two kinds of processes; collision and propagation. The collision is usually implemented as a set of predefined rules mapping pre- to postcollision states while obeying particle and momentum conservation. Frisch et al. (1987) showed that on macroscopic scales with length scales large compared to the node distance and timescales large compared to the collisional relaxation time, the dynamics of such a particle ensemble is adequately described by the incompressible Navier–Stokes equations. Thus, it is possible to simulate incompressible Navier–Stokes problems using LG methods. Further investigations in the last years have shown that LG methods are a valuable extensions of 'standard' discretization methods for flow problems, especially for porous media and multi-phase flow. On the other hand, they are not well suited for high Reynolds number flow because (in addition to other problems) the minimum viscosity (implicitly defined by the collision rules) is quite large leading to a prohibitive number of degrees of freedom compared to state-of-the-art methods. Having studied the properties of LG methods there have been numerous attempts to improve the original approach leading to a variety of so-called Lattice–Boltzmann (LB) methods, one of which was used in this work.

In order to see the difference between LB-methods and well-known Navier–Stokes discretizations we will give a short theoretical overview over the first technique. The reader interested in detailed information is referred to the cited literature.

The Boltzmann equation

$$\frac{\partial f}{\partial t} + \mathbf{v}\nabla f = \Omega, \tag{1}$$

used in statistical physics describes the dynamics of a continuous normalized particle distribution function $f(\mathbf{x}, \mathbf{v}, t)$, which is the probability to find a particle with microscopic velocity $\mathbf{v}(\mathbf{x}, t)$. The collision operator Ω contains details of the physical interaction between particles and can be of arbitrary complexity. The first step in order to construct a LB model is to discretize the microscopic velocity space with a discrete set of vectors $\mathbf{e}_i$ resulting in a so-called Lattice–Boltzmann equation

$$\frac{\partial f_i(\mathbf{x}, t)}{\partial t} + \mathbf{e}_i \nabla f_i(\mathbf{x}, t) = \Omega_i(f_i)(\mathbf{x}, t)_j, \quad i, j \in \{1, \ldots, n\}, \tag{2}$$

which, in fact, is a system of n first-order PDEs coupled via Ω_i, as will be seen below. It is known from statistical physics that for a collision operator of minimum complexity to generate fluid behavior the so-called single time relaxation approximation (STRA) form can be introduced

$$\Omega_i = -\frac{1}{\tau}(f_i - f_i^{\mathrm{eq}}), \tag{3}$$

which is readily interpreted as a source term resulting from the deviation of f_i from an equilibrium function f_i^{eq} which still has to be defined and τ is a microscopic relaxation time. The introduction of the minimum set of macroscopic fluid variables (i.e. velocity $\mathbf{u}$ and density ρ) is done by defining

$$\rho = \sum_{i=1}^{n} f_i, \qquad \mathbf{u} = \frac{1}{\rho}\sum_{i=1}^{n} f_i \mathbf{e}_i \tag{4}$$

and furthermore making an Ansatz for the equilibrium distribution f_i^{eq} of the form

$$f_i^{eq} = \rho[A_i + B_i(\mathbf{e}_i\mathbf{u}) + C_i(\mathbf{e}_i\mathbf{u})^2 + D_i\mathbf{u}^2] \tag{5}$$

with constants A_i, B_i, C_i and D_i still to be defined. The Lattice–Boltzmann equation (2) can now be discretized in space and time, e.g. via a first-order FD scheme resulting in

$$f_i(\mathbf{x}_k + \mathbf{e}_i\delta t, t + \delta t) = f_i(\mathbf{x}_k, t) + \Omega_i(\mathbf{x}_k, t). \tag{6}$$

This set of $k \times i$ equations can be interpreted as a system of evolution equations for a set of particle distribution functions f_i evaluated on nodes $\mathbf{x}_k$ of a uniform lattice with lattice spacing δh mimicking particle collision at these nodes and particle propagation to neighbouring nodes located at $\mathbf{x}_k + \mathbf{e}_i\delta t$ during δt. Usually, δh and δt are set to unity. Demanding that

$$\sum_{i=1}^{n} \Omega_i = \sum_{i=1}^{n} \Omega_i \mathbf{e}_i = 0, \tag{7}$$

implying a conservation of mass and momentum it can be shown that a multiscale Chapman–Enskog expansion of the kinetic moments of the set of f_i allows to choose appropriate coefficients in Eq. (5) in order to obtain a set of equations for the dynamics of the macroscopic fluid properties. These equations can (in the low Mach number limit $|\mathbf{u}| \ll c_s$ with a speed of sound c_s) be proven to be the incompressible Navier–Stokes equation

$$\frac{\partial(\mathbf{u})}{\partial t} + \mathbf{u}\nabla\mathbf{u} = -\frac{1}{\rho_0}\nabla p_\infty + \nu\nabla^2(\rho\mathbf{u}), \tag{8}$$

where p_∞ is the incompressible pressure and ρ_0 is the conserved initial mean density, the continuity equation

$$\frac{\partial\rho}{\partial t} + \nabla(\rho\mathbf{u}) = 0 \tag{9}$$

and an equation of state

$$p_\infty = c_s^2\rho. \tag{10}$$

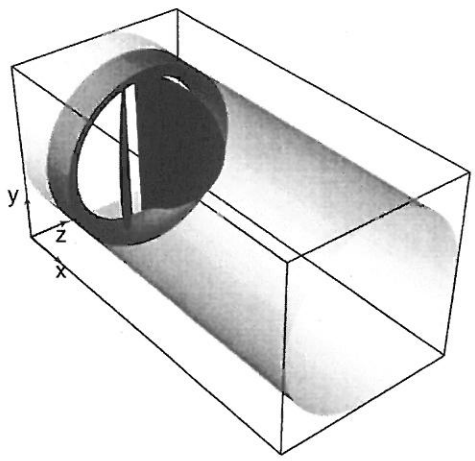

Fig. 1. View of the valve geometry used for simulation.

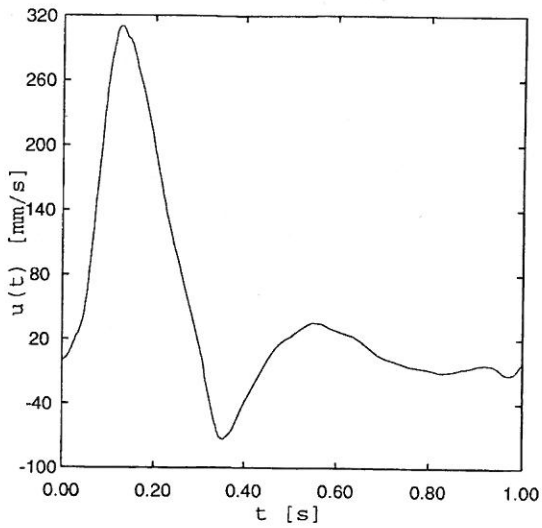

Fig. 2. Time-dependant maximum velocity boundary condition at the center of the tube.

For the simulations presented here we used a 3D cubic grid with nodes connected to their neighbouring nodes by grid vectors $\mathbf{e}_i\delta t$ ($\delta t = 1$) given by the $n = 15$ columns of the matrix (in units of δh)

$$\hat{N} = \begin{pmatrix} 0 & 1 & -1 & 0 & 0 & 0 & 0 & 1 & -1 & 1 & -1 & 1 & -1 & 1 & -1 \\ 0 & 0 & 0 & 1 & -1 & 0 & 0 & 1 & -1 & 1 & -1 & -1 & 1 & -1 & 1 \\ 0 & 0 & 0 & 0 & 0 & 1 & -1 & 1 & -1 & -1 & 1 & 1 & -1 & -1 & 1 \end{pmatrix},$$

where f_1 represents the probability distribution of resting particles. The speed of sound for the 3D cubic grid can be computed to be $c_s = \frac{1}{\sqrt{3}}\delta h/\delta t$ and the kinematic viscosity ν is related to the relaxation time τ via

$$\nu = \frac{2\tau - 1}{6}\frac{\delta h^2}{\delta t} \qquad (\tau > 0.5) \tag{11}$$

when using the so-called 3DQ15 model (Chen et al., 1991), where the equilibrium distributions are defined as

$$f_i^{eq} = \rho(\tfrac{1}{8} - \tfrac{1}{3}\mathbf{uu}),$$
$$f_i^{eq} = \rho(\tfrac{1}{8} + \tfrac{1}{3}(\mathbf{e}_i\mathbf{u}) + \tfrac{1}{2}(\mathbf{e}_i\mathbf{u})^2 - \tfrac{1}{6}\mathbf{uu}), \quad i \in \{2, \dots, 7\}, \tag{12}$$
$$f_i^{eq} = \rho(\tfrac{1}{64} + \tfrac{1}{24}(\mathbf{e}_i\mathbf{u}) + \tfrac{1}{16}(\mathbf{e}_i\mathbf{u})^2 - \tfrac{1}{48}\mathbf{uu}), \quad i \in \{8, \dots, 15\}.$$

Numerical experiments have shown (e.g. Noble et al., 1995) that under certain assumptions such an LB scheme can be tuned to give second-order convergence in space and linear convergence in time with respect to the exact solution of the corresponding Navier–Stokes problem.

3. Simulation properties

The geometry of the simulated flow problem is shown in Fig. 1. We simplified the problem by assuming the leaflets as being fixed and chose distinct opening angles between the leaves of the valve and the xy-plane ($z = 0$), dividing the tube vertically. We simulated one testcase with an angle of 40°, the other one with 12° corresponding to a maximum opening of the valve. The diameter of the tube is taken to be 20 mm, the length is 40 mm. Using

$$u_{peak} = 300 \text{ mm s}^{-1}, \qquad \nu = 3.3 \text{ mm}^2 \text{ s}^{-1} \tag{13}$$

results in a peak Reynolds number of 1818. We tested two different sets of boundary conditions. In the first case the flow enters the tube along the x-axis with a fully developed parabolic velocity profile of a time-dependant maximum amplitude shown in Fig. 2 (Stettler et al., 1981), the velocity BC was set by evaluating $f_i = f_i^{eq}$ at $x = 0$ according to Eq. (12) and was identical to the BC at the outlet.

As the existence of a fully developed parabolic profile at inlet and outlet has been questioned, a somewhat more sophisticated set of BC was alternatively applied. One possible and rather natural choice is to force the fluid to enter with a transient velocity profile constant along y and z. In addition, we set at the inlet $\partial p/\partial x = 0 \equiv \partial \rho/\partial x = 0$ (see Eq. (10)) by first computing the actual density of the nodes of the neighbouring plane downstream in each timestep and then plugging this density with the transient velocity value into Eq. (12) to obtain the desired f_i. At the outflow we analogously set a constant pressure value and $\partial \mathbf{v}/\partial x = \mathbf{0}$. We found that the system with this set of BCs (adapted from Filippova) behaved very similar to the system forced with parabolic inflow BCs apart from a few grid planes in the vicinity of the in- and outflow planes. The largest deviations in the maximum shear stresses were about 5%. Additionally, the second type of BCs result in a larger flux down-stream because the incoming velocity profile along the y–z plane is steeper in the vicinity of the cylinder walls. Basically, all kinds of Dirichlet or Neumann BC used in standard CFD methods can be constructed analogously for LB schemes.

The computational domain of the results shown here consists of $280 \times 140 \times 140$ grids nodes. All nodes beyond the 'wall' nodes discretizing the cylinder surface were essentially ignored during the numerical computation. Additionally, we tested a grid of $360 \times 160 \times 160$ nodes to extend the distance between inflow plane, valve and outflow plane, but again the results were almost identical. As the collision procedure is purely local and the propagation step implies next-neighbor calculations, the algorithm takes advantage of computing in parallel equally sized subdomains obtained by geometric domain decomposition. At every timestep all relevant distributions of the boundary nodes of each subdomain are

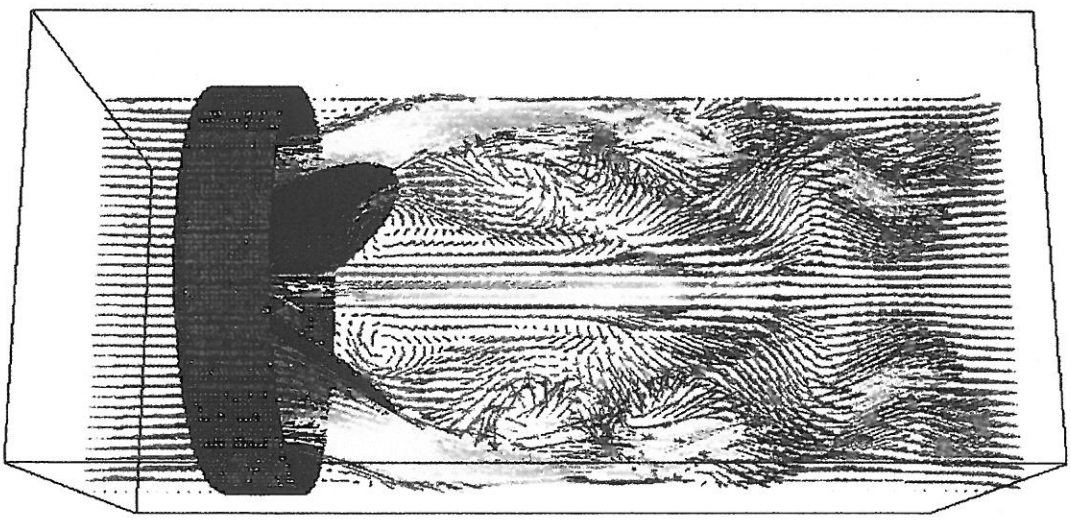

Fig. 3. Velocity vector plot at $t = 0.15$ s.

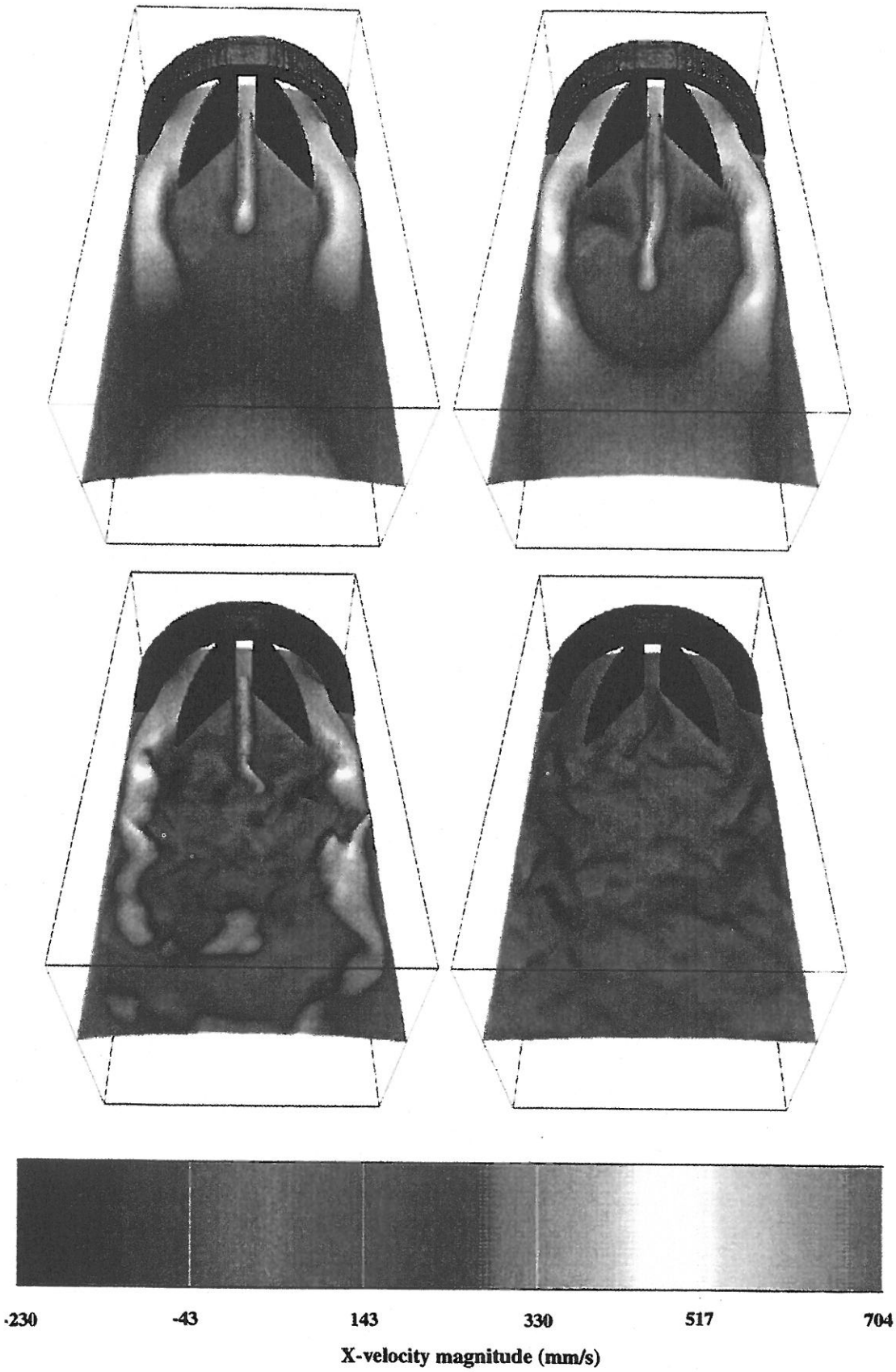

Fig. 4. Transient dynamics from left to right and top to bottom: $t = 0.117, 0.133, 0.173, 0.282$ s.

communicated via message passing to the corresponding neighbouring subdomains. No-slip conditions ($\mathbf{u} = \mathbf{0}$) on the wall nodes are applied by swapping all anti-parallel distributions f_i and f_j for which $\mathbf{e}_i + \mathbf{e}_j = \mathbf{0}$ in every time-step (so-called bounce-back rule). The code is implemented on an HP workstation cluster, on a 16-processor PARSYTEC parallel computer based on a power-PC architecture using the message-passing software

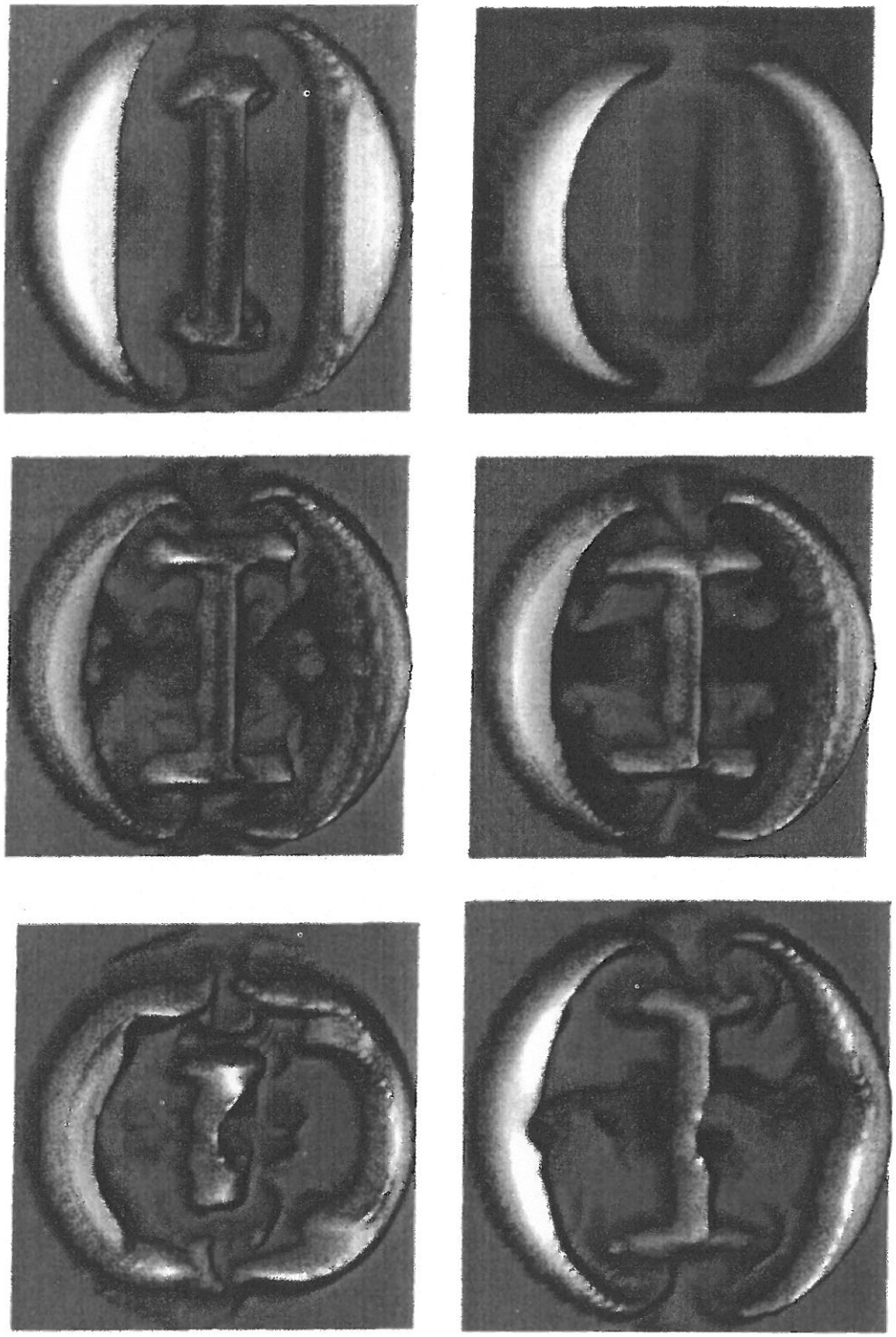

Fig. 5. Transient dynamics for different slicing planes and constant time (left) and different time and constant slicing planes (right column), see text for details.

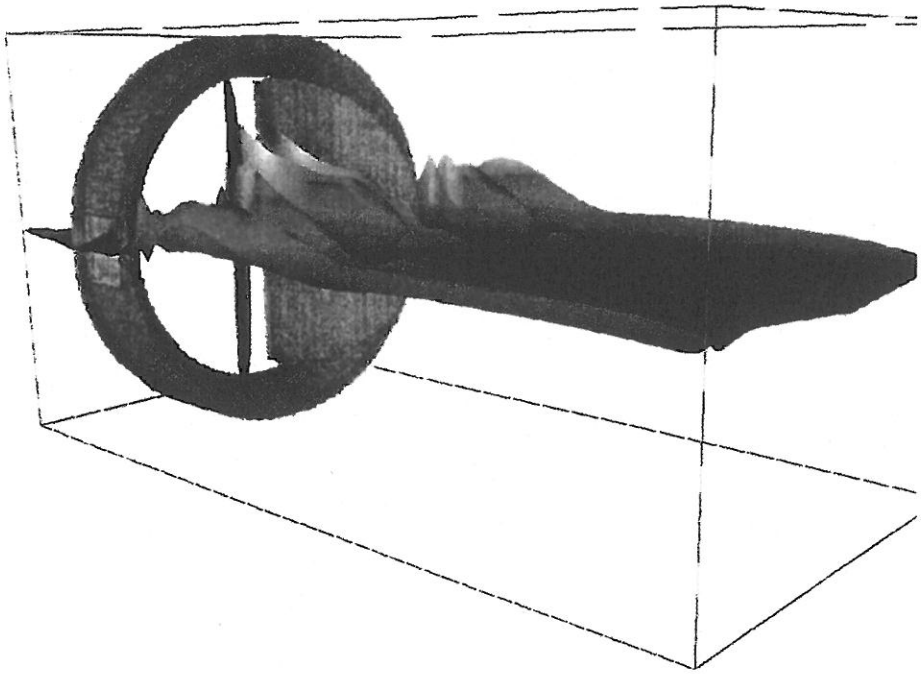

Fig. 6. Contour plot of $|\sigma_{xz}|$ at $t = 0.113$ s.

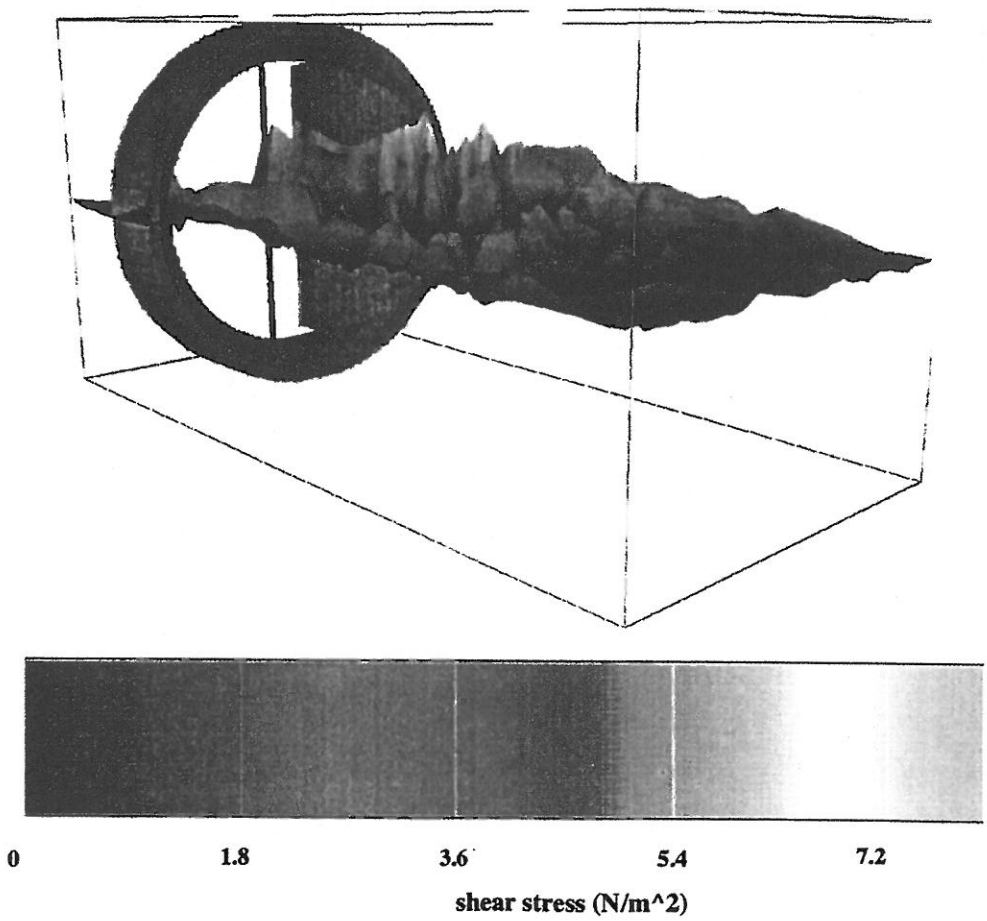

Fig. 7. Contour plot of $|\sigma_{xz}|$ at $t = 0.165$ s.

PVM[1] and on a Fujitsu VPP 700 vector supercomputer. The computation time for the simulation of the first 0.5 s of the cardiac cycle was about 20 h on *one* processor of the Fujitsu VPP 700.

4. Numerical results

The simulated pulsatile flow shows a very complicated, inherently three-dimensional behavior which is difficult to visualize appropriately. To get a first and limited impression of the flow, Fig. 3 shows a velocity vector plot of a mid-plane at time $t = 0.15$ s where the flow starts to become three dimensional. The arrows are colored according to the magnitude of the downstream velocity component (colormap is identical to Fig. 4). All post-processing was done using the AVS software package.[2] Fig. 4 shows contour plots of u_x in the xz-plane ($y = 10$ mm) bisecting the tube while the system becomes unstable. In order to get an impression of the symmetry breaking process, Fig. 5 shows on the left column contour plots of u_x at $t = 0.141$ s for different yz-planes (from top to bottom: $x = 11.1$, 16, 23.1 mm) and on the right column for the yz-plane with $x = 16$ mm at different times (from top to bottom: $t = 0.10$, 0.125, 0.,141 s). The color legend is again identical to Fig. 4. Basically, the impinging vertical 'jet' is quenched by the top and bottom pairs of spiral vortices forcing the system to an initial symmetry breaking, resulting in a weakly turbulent flow decreasing to an almost resting state after about 0.5 s. As we were especially interested in local peaks of the velocity gradient, we just computed the acceleration phase of the cardiac cycle.

An important issue for valve hemodynamics analysis are shear stress levels in the fluid. We measured the magnitude of $\sigma_{xz} = \nu\rho(\partial u_x/\partial z - \partial u_z/\partial x)$ and found shear stress peaks in the vicinity of the entrance region of about $10\ \mathrm{N\,m^{-2}}$. Somewhat surprisingly we observed shear stresses of similar size far away from the walls which turned out to be reasonable because of very steep velocity gradients due to vortex–jet interactions. Figs. 6 and 7 show contour plots of $|\sigma_{xz}|$ in the xz-plane ($y = 10$ mm) bisecting the tube at times $t = 0.113$ and 0.165 s, Fig. 8 shows the absolute value of $|\sigma_{xz}|$ plotted along the z-axis for $x = 5.7$ mm (valve inlet) and $y = 10$ mm corresponding to Fig. 6, analogously Fig. 9a and b show $|\sigma_{xz}|$ plots for $t = 0.165$ s, $y = 10$ mm, with $x = 5.7$ and 16.8 mm, respectively, corresponding to Fig. 7. The simulation with the manufacturers predefined maximum leaflet opening angle of 12° gave quantitatively similar results and is thus omitted. The authors believe that the simulation of fixed leaflets with a maximum opening angle still is a reasonable lower estimate for the maximum shear stress during one cycle.

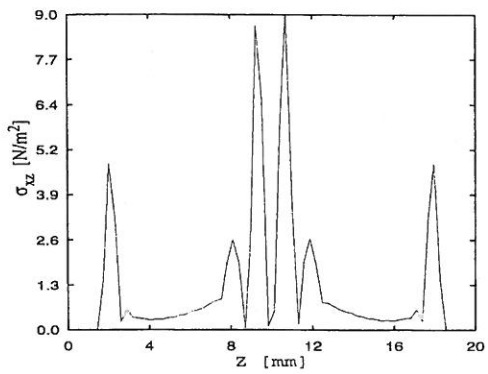

Fig. 8. $|\sigma_{xz}|$ at $t = 0.113$ s, $x = 5.7$ mm, $y = 10$ mm.

5. Discussion

Our primary goal was to test the suitability of LB methods for 3D bioengineering pulsatile flow problems. The resulting flow dynamics could not be compared to actual experiments in details, but the resulting shear stresses were of the same order of magnitude as observed in experiments of similar *in vitro* flow problems (e.g. Lee et al., 1995; Sakhaeimanesh et al., 1996) and are well below the critical shear stress range to cause necrosis of red blood cells or lethal erythrocyte and thrombocyte damages. However, one has to keep in mind that short-time shear stress peaks are to be expected right before the closure of the valve leaflets. It is our conviction that this regime can only be studied with sufficient accuracy when allowing for a dynamic fluid-structure coupling (moving leaflets). The extension of the LB method to include such fluid-structure interaction bears no fundamental difficulties but requires further research and an enormous implementation effort. The use of a uniform grid decreases the possibilities of the present algorithm to model the detailed influence of leaflets with varying thicknesses and other geometric details which are, nevertheless, important for the accurate prediction of local peak stress fields in the moment of valve closure. On the other hand, it turned out that in order to follow the development of instabilities a high geometric resolution even far away from the walls is necessary. In this respect the study may give a hint that manually refined meshes in standard discretization methods requiring *a priori* conjectures about zones of steep velocity gradients (typically, only conjectured in the near vicinity of the valve leaflets) could result in a lack of bulk flow resolution. Only fully adaptive schemes controlled by a posteriori error estimation (Becker et al., 1995) could provide meshes with better

[1] see e.g. web page at *http://www.avs.com.*

[2] see e.g. web page at *http:/www.epm.ornl.gov:80/pvm.*

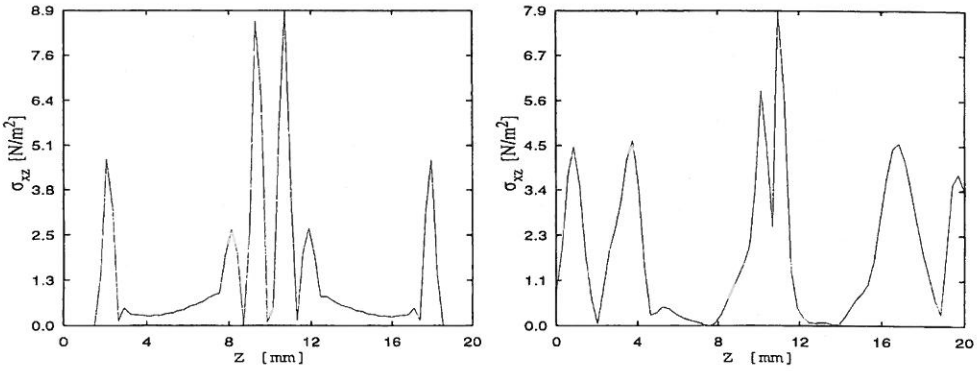

Fig. 9. $|\sigma_{xz}|$ at $t = 0.165$ s, $y = 10$ mm, left: $x = 5.7$ mm, right: $x = 16.8$ mm.

global resolution than the uniform grid used in this study. The evolving dynamics of the blood flow in this study resulting in a loss of symmetry and slightly turbulant flow are well intelligible and seem to be intrinsic properties of the chosen geometry and material parameters. They thus give a hint that the leaf topology is still by far not optimal to allow for laminar flow, especially when taking into account, that the Reynolds number for maximum physiological flows can be three or four times higher than in this study. Despite the neglection of effects like dynamic fluid-flow coupling, artery elasticity effects or non-Newtonian stress–strain relationships, the computation presented here using the LB method gave reasonable results for the prediction of velocity and stress fields. Thus, it could contribute answers to questions concerning the complex dynamics of blood flows in semi-turbulent flow regimes of aortic valve devices additionally to structurally easier problems like stenosis, aneurysm- and bifurcationdominated blood flow dynamics. We found that LB-methods are suitable to solve complex and large-scale transient problems. This observation is supported by other works (e.g. Chen et al., 1992). Finally, it should be pointed out, that more advanced discretizations could be used to solve Eq. (2). Only extended (ongoing) work in this direction will solve the question if and when it is advantageous to solve a coupled set of *first-order* LB equations rather than the *second-order* Navier–Stokes equation.

Acknowledgements

The first author wants to acknowledge the support provided by the State of North-Rhine Westfalia for support during the research program 'Simulation and Visualization'. The second author wants to acknowledge the support provided by the Council for Scientific Humanistic Development (CDCH, Venezuela) in the framework of the Cardioma Project and the National Council for Scientific Research (CONICIT, Venezuela).

References

Barjet, H., 1983. Haemodinamique, Amep, Paris.

Becker, R., Johnson, C., Rannacher, R., 1995. Adaptive error control for Multigrid FE methods. Computing 55, 271–288.

Benzi, R., Succi, S., Vergassola, M., 1992. The Lattice–Boltzmann equation: theory and application. Physics Reports (Review Section of Physics Letters) 222(3), 145–147.

Braunwald, E., 1992. Heart Disease Textbook of Cardiovascular Medicine, Saunders, New York.

Cerrolaza, M., Herrera, M., Berrios, R., Annicchiarico, W., 1997. A comparison of the hydrodynamical behaviour of three heart aortic prostheses by numerical methods. Journal of Medicine Engineering and Technology (to appear).

Chandran, K.B., Cabel, G.N., Khalighi, B., Chen, C.J., 1985. Laser anemometer measurements of pulsatile flow past aortic valve prostheses. Journal of Biomechanics 16(10), 865–873.

Chandran, K.B., Khalighi, B., Chen, C.J., 1985. Experimental study of physiological pulsatile flow past valve prostheses in a model of human aorta–II. Tiling disc valves and the effect of orientation. Journal of Biomechanics 18(10), 773–780.

Chen, S., Chen, H., Martinez, D.O., Matthaeus, W.H., 1991. LB model for simulation of magnetohydrodynamics. Physics Review Letters 67.

Chen, S., Wang, Z., Shan, X., Doolen, G., 1992. LB-CFD in Three Dimensions. Journal of Statistical Physics 68, 34.

Drobinsky, G., Eugene, M., 1992. Exploration Haemodinamique Cardiovasculaire, Masson, Paris.

Farahifar, D., Cassot, F., Bodard, H., 1985. Velocity profiles in the weak of two prosthetic heart valves using a new cardiovascular simulator. Journal of Biomechanics 18(10), 789–802.

Filippova, O., private Communications.

Frisch, U., Humières, D., Hasslacher, B., Lallemand, P., Pomeau, Y., Rivet, J.P., 1987. Lattice Gas hydrodynamics in two and three dimensions. Complex System 1, 649.

Gokhale, V.V., Tanner, R.J., Bischoff, K.B., FE solution for the Navier–Stokes equations for a 2D steady flow through a section of a canine aorta model. Journal of Biomechanics 11, 241–249.

Imaeda, K., Goodman, F., Analysis of non-linear pulsatile flow in arteries. Journal of Biomechanics 13(8), 1007–1022.

Lee, S.C., Chandran, K.B., 1995. Numerical simulation of instantaneous backflow through central clearance of . . . . Medical and Biological Engineering and Computers 33, 257.

Noble, D.R., Chen, S., Georgiadis, J.G., Buckius, R.O., 1995. A consistent hydrodynamic boundary condition for the LB method. Physics Fluids 7, 203.

Quian, Y.H., D'Humieres, D., Lallemand, P., 1992. Lattice BGK models for Navier–Stokes equation. Europhysics Letters 17(6).

Rosseau, E.P.M., Van de Ven A.P.C., Van Steenhoven, A.A., Seroo, J.M., 1984. Design of a system for the accelarated loading of heart valve prostheses. Journal of Biomechanics 17(2), 145–153.

Sakhaeimanesh, A.A., Morsi, Y., Tansley, G., 1996. In: Proceedings of the 10th Conference of the European Society of Biomechanics (Ed.), van der Sloten et al., J., Leuven, Belgium.

Sallam, I.A., Shaw, A., Bain, W.H., 1976. Experimental evaluation of mechanical haemolysis with Starr-Edwards, Kay-Shiley and Bjork-Shiley valves. Scandinavian Journal of Thoracic and Cardiovascular Surgery 10, 117–122.

Sikarskie,, D.L., Stein, P., Vable, M., 1979. A mathematical model for aortic valve vibration. Journal of Biomechanics 17(11), 831–837.

Skalak, R., 1982. Finite elements in biofluid mechanics. FE Analysis in Biomechanics.

Stevenson, D.M., Yoganathan, A.P., 1985. Numerical simulation of steady turbulent flow through trileaflet aortic heart valves – I. Computational scheme and methodology. Journal of Biomechanics 18(12), 899–907.

Stettler, J.C., Niederer, P., Anliker, M., Casty, M., 1981. Theoretical analysis of arterial hemodynamics .... Annals of Biomedical Engineering 9.

Tillman, W., Reul, H., Herold, M., Bruss, K.H., Van Gilse, J., 1984. *In vitro* wall shear measurements at aortic valve prostheses. Journal of Biomechanics 17(4), 263–279.

Woo, Y.R., Yoganathan, A.P., 1986. *In vitro* pulsatile flow measurements in the vincinity of mechanical heart in the mitral flow chamber. Life Support Systems 4, 115–139.

Yoganathan, A.P., Corcoran, W.H., Harrison, E.C., 1979. *In vitro* velocity measurements in the vicinity of aortic prostheses. Journal of Biomechanics 12, 135–152.